Earth and Space Science

RESEARCH ARTICLE
10.1029/2024EA003619

Evaluation of Modeled Diurnal Warming Estimates for Application to Producing Sea Surface Temperature Analyses

Gary A. Wick[1], Sandra L. Castro[2], Andrew Harris[3], and Jonathan Mittaz[4]

[1]NOAA Physical Sciences Laboratory, Boulder, CO, USA, [2]Colorado Center for Astrodynamics Research, University of Colorado, Boulder, CO, USA, [3]NOAA Cooperative Institute for Satellite Earth System Studies, Earth System Science Interdisciplinary Center, University of Maryland, College Park, MD, USA, [4]Department of Meteorology, University of Reading, Reading, UK

Key Points:

- A preferred configuration of a mixed-layer ocean model is found to predict diurnal warming from global numerical weather prediction output
- The predictions reproduce the observed range and distribution of diurnal warming from geostationary satellites but with notable scatter
- The same configuration also favorably reproduces observations from research cruises and outperforms other models

Correspondence to:
G. A. Wick,
gary.a.wick@noaa.gov

Citation:
Wick, G. A., Castro, S. L., Harris, A., & Mittaz, J. (2024). Evaluation of modeled diurnal warming estimates for application to producing sea surface temperature analyses. *Earth and Space Science*, *11*, e2024EA003619. https://doi.org/10.1029/2024EA003619

Received 1 MAR 2024
Accepted 6 AUG 2024

Author Contributions:

Conceptualization: Gary A. Wick
Investigation: Gary A. Wick, Sandra L. Castro, Andrew Harris
Methodology: Gary A. Wick, Sandra L. Castro, Andrew Harris, Jonathan Mittaz
Software: Gary A. Wick, Jonathan Mittaz
Visualization: Gary A. Wick, Sandra L. Castro
Writing – original draft: Gary A. Wick
Writing – review & editing: Gary A. Wick, Sandra L. Castro, Andrew Harris, Jonathan Mittaz

Abstract Accurate knowledge of the amount of diurnal warming present in sea surface temperature (SST) observations at different times and effective depths is important for multiple applications including the production of blended SST analyses. This work explores the ability of a modified Kantha-Clayson-type one-dimensional mixed layer ocean model with wave effects to accurately simulate the observed diurnal warming amplitude over a global grid when forced with coarse resolution numerical weather prediction (NWP) outputs. The sensitivity of the modeled diurnal amplitudes to multiple adjustable parameters and model configurations is evaluated to determine whether a preferred configuration can be identified that yields reliable predictions. The accuracy of the predictions is determined through comparison against estimates from operational SST retrievals from geostationary satellites. The results show that a single configuration can yield predictions that reproduce the observed range of diurnal warming amplitudes across a range of seasons and locations and an accurate occurrence frequency of the largest amplitude events. Simulated amplitudes fall along the one-to-one line with observations but with significant scatter due to factors including positioning of the NWP fluxes. The identified configuration is also shown to favorably reproduce diurnal warming observations from multiple research cruises. Overall uncertainty of the simulated diurnal warming amplitude across the different tests ranges between 0.4 K for all observations to ∼1 K for the largest warming events. While the focus is not on model comparisons, the results show improved performance relative to other models. Use of the model appears warranted but the associated uncertainty must be considered.

Plain Language Summary Production of accurate maps of the daily sea surface temperature require observations to be adjusted for differing amounts of warming from the sun during the day. Different configurations of a model for this warming at the ocean surface are tested to see if the model can match the warming seen in satellite data when given outputs from weather forecast models. One configuration is found that gives good predictions of the range of observed warming amounts and the frequency with which they occur in different regions and seasons, but predictions at specific locations still show differences with the observed values. This same version of the model is also able to reasonably reproduce observations of the warming from research ships and performs better than some other available models. The results suggest that this new model can be successfully used to improve SST products but that users must understand the uncertainty remaining in the predictions.

1. Introduction

Diurnal warming of the water near the ocean surface occurs under conditions of low wind speeds with sufficient levels of solar radiation. While the typical daily amplitude of diurnal warming across the oceans is of O(0.5 K) or less (e.g., Kawai & Wada, 2007; Kennedy et al., 2007; Stuart-Menteth et al., 2003), under very low wind speeds it can be significantly larger. Warming in excess of 5 K at depths of 0.3–0.6 m has been observed with in situ observations (Flament et al., 1994) and several recent studies using satellite data have found that warming of 5 K or more is not uncommon (e.g., Gentemann et al., 2008; Merchant et al., 2008; Pisano et al., 2022; Wick & Castro, 2020). Additional factors impacting the near-surface density structure including fresh layers from precipitation and river outflows can also enhance diurnal heating (e.g., Shackelford et al., 2022; Thompson et al., 2019).

The warming and associated near-surface temperature gradients are important for several reasons including modulation of air-sea heat fluxes and impacts on climate variability. The effect of diurnal variability on air-sea

fluxes has been discussed in many studies including those by Halpern and Reed (1976), Price et al. (1986), Fairall, Bradley, Godfrey, et al. (1996), Li et al. (2001), Danabasoglu et al. (2006), Clayson and Bogdanoff (2013), Weihs and Bourassa (2014), and Marullo et al. (2016). Other studies have documented the impact of diurnal warming on forecasting (e.g., Brunke et al., 2008), convection (e.g., Bellenger et al., 2010; de Szoeke et al., 2021), intra-seasonal variability (Bernie et al., 2005, 2007; McCreary et al., 2001; Shinoda, 2005; Shinoda & Hendon, 1998; Yang & Slingo, 2001), evolution of the El Niño Southern Oscillation (ENSO, e.g., Ham et al., 2010; Masson et al., 2012; Tian et al., 2019), and predictability of the Madden-Julian oscillation (e.g., Seo et al., 2014; Woolnough et al., 2007). Kawai and Wada (2007) further discussed the various impacts of diurnal sea surface temperature (SST) variability in their review.

One specific application requiring compensation for the near-surface diurnal warming is the production of daily blended Level 4 (L4) SST analyses. These analyses (see e.g., Castro et al., 2016; Dash et al., 2012; Martin et al., 2012; Vazquez-Cuervo et al., 2022 for summaries and comparisons) combine observations from multiple sensors in an effort to take advantage of the strengths of the different data types and produce gap-filled SST products with improved accuracy characteristics. These are among the most widely utilized SST products because of their spatial completeness and ease of use. The observations, however, can be drawn from both in situ and satellite-borne sensors and have different measurement times and effective sampling depths. Diurnal warming causes differences between the sampled temperatures, and blending the data to provide a single estimate representative of a specific time and depth or, alternatively, the "foundation" temperature representing the value at a depth notionally free from any diurnal warming (see, e.g., Donlon et al., 2007), requires some method or assumptions to account for these differences.

Various models with differing complexity have been developed to predict the amplitude and evolution of diurnal warming. In past reviews and evaluations (e.g., Karagali et al., 2017; Kawai & Wada, 2007; Zhang et al., 2018), the models have commonly been grouped into categories based on complexity including turbulence or diffusion models (e.g., Kantha & Clayson, 1994; Noh & Kim, 1999, and the Generalized Ocean Turbulence Model, GOTM, Burchard et al., 1999), bulk or slab models (e.g., Fairall, Bradley, Godfrey, et al., 1996; Price et al., 1986; Zeng & Beljaars, 2005), and simple parameterizations (e.g., Clayson & Weitlich, 2007; Gentemann et al., 2003; Price et al., 1987; Webster et al., 1996). Several models have received particular attention. The COARE (Coupled Ocean Atmosphere Response Experiment) warm layer model (Fairall, Bradley, Godfrey, et al., 1996) is commonly used in air-sea flux applications and refinements have been proposed by Wick et al. (2005) and Gentemann et al. (2009). Work within NOAA is now exploring integration of the model within the unified forecast system and Near Surface Sea Surface Temperature (NSST) analysis (e.g., Zhou et al., 2022). The Zeng and Beljaars (2005) model and derivatives proposed by Takaya et al. (2010), Large and Caron (2015), and Akella et al. (2017) have been evaluated for inclusion in climate and numerical weather prediction (NWP) forecast models. GOTM has been shown to exhibit skill in accurately reproducing high-resolution observations of diurnal warming in several analyses (e.g., Giglio et al., 2017; Hallsworth, 2005; Karagali et al., 2017; Pimentel et al., 2008; Schackelford et al., 2022).

While these studies have established the successful potential of the diurnal warming models under specific circumstances, demonstrating their consistent performance over globally varying conditions and extremes has been more challenging. Recent studies have begun to explore their capabilities over broader ranges of conditions. Karagali et al. (2017) extended testing with GOTM to multiple distinct locations with success, and Pimentel et al. (2019) demonstrated good performance of GOTM relative to satellite-based observations from the Mediterranean Sea. Zhang et al. (2018) tested multiple diurnal warming models against satellite observations over the extended tropical warm pool region. Luo et al. (2022) additionally tested various models against an extended series of ship-based observations in the Caribbean. The results exhibit differences, however, and a firm understanding of the expected uncertainties of diurnal warming estimates over global extents is still not complete. The ability of the models to accurately reproduce the largest magnitude (>3 K amplitude) diurnal warming events, in particular, requires more dedicated investigation.

Within the systems developed to construct the blended L4 SST analyses, the approaches to treating diurnal warming have generally been simple. A common approach in analyses of the foundation temperature has been to either use only nighttime observations (Chin et al., 2017; Høyer et al., 2013) or exclude daytime observations below a wind speed threshold of ∼6 m/s (e.g., Brasnett, 2008; Good et al., 2020; Martin et al., 2012) when diurnal heating is expected. The community is now showing interest in exploring more complex approaches and diurnally resolved analyses (While et al., 2017) are also emerging.

Various efforts in constructing SST analyses and reconciling different temperature measurements have begun to specifically examine the potential for broader use of the Kantha-Clayson model (first described in Kantha and Clayson (1994) with recent variations incorporating wave effects, Kantha & Clayson, 2004). Versions of the original model were incorporated in early efforts to blend SST observations at the UK Met Office (e.g., Horrocks et al., 2003) and in efforts to improve retrievals of the temperature at depth from geostationary satellites (Wick et al., 2002). The model has also been employed in the time and depth adjustment of SST estimates within production of an SST climate data record under the framework of the European Space Agency Climate Change Initiative (Embury et al., 2012; Merchant et al., 2019). Recently, a derivative of the model with wave effects was ported into Fortran 90 at the NOAA National Environmental Satellite Data and Information Service (NESDIS) Center for Satellite Applications and Research (STAR) and implemented in a version of NOAA's operational Geo-Polar Blended SST Analysis (Maturi et al., 2017) to explicitly adjust satellite SST retrievals to a foundation temperature prior to merging. This code has additionally been shared with the European Organisation for the Exploitation of Meteorological Satellites (EUMETSAT), which has expressed interest in applying the model as part of their validation workflow. It is this general version of the model that is employed in this study with access as described in the Data Availability Statement.

The versions of the Kantha-Clayson-type models implemented for these uses have various parameters that are tunable and/or can be configured. While some basic testing has been performed for the applications discussed above, the impact of adjustments to, and selection of, these parameters can be significant and has, to date, not been fully investigated. Optimum utilization of the model within these emerging applications requires more careful and systematic analysis of the sensitivity to these parameters and the resulting uncertainties in the predicted diurnal warming.

The primary objective of this paper is to quantitatively evaluate different configurations of a modified version of the Kantha-Clayson model with wave effects (Kantha & Clayson, 2004; hereafter KC04) with a specific focus on the case where the model is forced with NWP model outputs to obtain diurnal warming estimates for application to blended SST production and validation. The initial operational application is to adjust for the amount of diurnal warming present in individual retrievals prior to merging, but the model can further be used to provide temporally varying estimates of the skin temperature from the analyzed foundation temperature. The accuracy and uncertainty of predicted amplitudes of daily diurnal warming obtained with different model parameters are derived through comparisons against satellite-derived diurnal warming estimates and guidance on recommended model configurations developed. The reliability and generality of those configurations found to perform well are then further tested with application to diverse observations from selected past research cruises. While the focus is on investigating the capabilities of the modified KC04 model and not selecting a specific model from the full range of available options, the corresponding results obtained using a small set of other common diurnal models are also included for comparison purposes. Background on the models employed and the data used for forcing and validation is provided in Section 2. Assessment of the model-derived diurnal warming amplitudes obtained using NWP forcing is described in Section 3. Further evaluation of those model configurations using high resolution research cruise data is presented in Section 4. Conclusions and recommendations are then summarized in Section 5.

2. Models and Data

As noted, a focus of this work is to explore the potential capabilities and limitations of different configurations of the modified KC04 model with wave effects for simulation of near-surface diurnal warming in support of current and planned activities within NOAA and EUMETSAT. The forcing data most relevant to these applications is large-scale, near-global, coarser resolution inputs such as derived from NWP model outputs. Validation of the derived diurnal warming predictions requires global-scale observations, and recent satellite-derived products serve as a principal candidate. In support of these goals, however, additional models will also be compared and different types of forcing and validation data will be utilized. Basic details on the different models and data sources employed are summarized in this section.

2.1. Modified Kantha-Clayson Model

The KC04 model introduced the contribution of near-surface turbulence due to wave breaking, Langmuir circulations, and Stokes drift to the one-dimensional, second moment turbulence closure mixed layer model of

Kantha and Clayson (1994). The model can further be classified as a level 2 1/4 closure model within the Mellor-Yamada hierarchy of models (Mellor & Yamada, 1974, 1982) with terms in the second moment turbulence closure equations derived from large eddy simulations. The model incorporates diagnostic equations for the temperature, salinity, velocity, turbulent kinetic energy, and turbulent length scale. Complete profiles of the temperature are simulated at each model time step. Additional modifications incorporated here, in the work of Wick et al. (2002), and in the implementation within the NOAA blended SST workflow to focus on simulation of the near-surface temperature structure include enhanced vertical resolution near the surface and the capability for exponential damping of turbulence immediately below the air-sea interface.

In all simulations, at each time step the model inputs the wind stress, and radiative and turbulent heat flux components. To account for wave effects, the model additionally inputs, when available, the significant wave height and primary wave period and direction. The simulations extend to a depth of 50 m with 140 levels that scale exponentially from 0.005 m within the top 0.025–1 m below 16 m. The absorption of solar radiation is presently parameterized using the well-known nine-band model of Paulson and Simpson (1981), which has fixed exponential depth scales and weighting coefficients, though further modified approaches are being evaluated independently. Additional implementation details specific to application to different data (e.g., time step, run duration, and interpretation of the amplitude of diurnal warming) are described below.

While designed to be consistently applicable across a wide range of conditions, as is common for a model of this type, the model incorporates several parameters that can be considered "tunable." Within the current implementation of the model, a configuration file allows selection of different mixing options and specification of the values for adjustable parameters. In addition to flags selecting inclusion of effects related to wave breaking, Langmuir mixing, and shear instability, the parameters include a background mixing rate, enhancement factors for shear-induced mixing and wave breaking effects, and sets of constants for the turbulence closure equations. The tests presented below examine the sensitivity to these parameters and associated accuracy of the diurnal warming predictions.

2.2. Additional Diurnal Warming Models for Comparison

Three additional models were employed to provide a comparison of the accuracy of simulated diurnal warming from the modified KC04 model and other potential approaches. These included the COARE warm layer (Fairall, Bradley, Godfrey, et al., 1996), the Zeng and Beljaars (2005), and the Takaya et al. (2010) models. They were selected for their broad usage for different applications including air-sea flux estimation and data assimilation. Each model is less computationally complex than the KC04 model and provides estimated diurnal warming amplitudes based on an assumed shape for the near-surface temperature profile. The comparisons are particularly relevant to establish whether the additional complexity of the modified KC04 model is warranted to provide improved global diurnal warming amplitude estimates. The COARE warm layer model used in this study was drawn from the version 3.6 release of the TOGA-COARE bulk air-sea flux algorithm (https://github.com/NOAA-PSL/COARE-algorithm), though the warm-layer component of the code was not significantly changed since version 2.0. While other studies (e.g., Karagali & Høyer, 2013) suggested the Zeng and Beljaars model (ZB hereafter) overestimates diurnal warming amplitudes in its original configuration, it was found to provide among the best results in the intercomparison by Zhang et al. (2018). The modified version by Takaya et al. (2010) was proposed as a refinement over ZB and is also tested here.

2.3. NWP Forcing Data

To provide global-scale diurnal warming amplitude estimates for use in the generation of near-real-time daily L4 SST analyses, consistent, timely, and complete forcing data are required throughout the globe. Outputs from global NWP weather forecast models are the most practical candidate. Based on the initial targeted application to generation of operational NOAA blended SST analyses, the tests here employ analysis outputs from the operational NOAA Global Forecast System (GFS) and Wave Watch III (Tolman et al., 2002) models. Both models are run four times daily with analysis times of 00, 06, 12, and 18Z. For the period of the study from July 2019 to March 2020 (see below) the operational version of the GFS model was v15.1 with a nominal grid resolution of approximately 13 km. All fields were mapped to a regular 0.5° grid in initial processing. Finer resolution is possible, but this selection was made to reduce processing time in the testing of multiple diurnal warming model configurations.

Specific parameters extracted from the GFS outputs include the six-hourly analyzed instantaneous values of the 10-m horizontal wind speed components, the surface latent and sensible heat fluxes, and the upwelling and downwelling components of the short- and long-wave radiative heat fluxes at the surface. While future applications may employ forecasted future values, the analyzed values were deemed most appropriate to evaluate the fundamental accuracy of the diurnal warming model's predicted daily amplitude. Values were extracted from the surface GRIB files downloaded regularly following the completion of each model run. The upwelling and downwelling radiative flux components were further combined to provide net solar and longwave radiative fluxes at the surface. Parameters extracted from Wave Watch III included the significant wave height and primary wave period and direction. Further details on how the parameters were input and utilized within the models are provided in Section 3 below.

2.4. Satellite Validation Data

To evaluate the modeled diurnal warming amplitude estimates across a broad range of representative environmental conditions, satellite-derived SST products were used as the primary source of validation data. The near-continuous sampling enabled by geosynchronous satellites provides the best resolution of the diurnal cycle of the skin SST, but the accuracy of SST retrievals from geosynchronous satellites has typically been poorer than that from polar orbiting satellites, complicating accurate estimation of the diurnal warming amplitude (e.g., Wick et al., 2002). Wick and Castro (2020), however, building on previous work using the Spinning Enhanced Visible and Infrared Imager (SEVIRI) by Le Borgne et al. (2012) and Karagali and Høyer (2014), demonstrated that the current operational SST retrievals from the SEVIRI on Meteosat-11, the Advanced Himawari Imager (AHI) on Himawari-8, and the Advanced Baseline Imager (ABI) on GOES-16 could provide diurnal warming amplitude estimates with sufficiently reliable accuracy, particularly for the largest amplitude events, when multiple potential contributions to the warming uncertainty were explicitly considered. The present study employs daily diurnal warming amplitude estimates derived using the "profile" methodology from Wick and Castro (2020) for the SEVIRI on Meteosat-11, the AHI on Himawari-8, and the ABI on GOES-16. While providing the smallest number of retrieved amplitudes, the profile approach derived from continuous sequences of valid SST retrievals across the diurnal cycle was found to yield the most reliable diurnal warming estimates of the methods considered. Daily amplitude estimates were derived for the months of July 2019, September 2019, January 2020, and March 2020.

2.5. Cruise Forcing and Validation Data

To further test and validate the large-scale results obtained with the diurnal warming models using NWP forcing, additional high-resolution measurements from selected research cruises were utilized. In all cases, the cruise data included the wind stress and heat fluxes at a temporal resolution of 10-min or better as derived from observations using the COARE bulk flux algorithm (Fairall, Bradley, Rogers, et al., 1996). The selected cruises include periods drawn from the Dynamics of the Madden-Julian Oscillation (DYNAMO) campaign as well as the Nauru and KWAJEX (Kwajalein Experiment) deployments contained within the extensive research cruise and air-sea flux archive developed and maintained by the NOAA Physical Sciences Laboratory (PSL) and its predecessor the Environmental Technology Laboratory (ETL). A final set of observations were taken from a data set collected aboard the NOAA R/V *Ronald H. Brown* including radiometric skin temperature measurements from the Calibrated Infrared In Situ Measurement System (CIRIMS; Jessup & Branch, 2008) and obtained from the Applied Physics Laboratory (APL) at the University of Washington. A summary of the cruise segments and relevant observation characteristics is included in Table 1.

3. Gridded Diurnal Warming Simulations With NWP Forcing

To evaluate the ability of the modified KC04 model to provide reliable, global estimates of the diurnal warming amplitude, the primary analysis focused on application of the model on a geographic grid with forcing from NWP-derived inputs. Testing examined the accuracy and sensitivity of simulated daily diurnal warming amplitudes to selected adjustable parameters and configurations through comparison against the diurnal warming estimates derived from geostationary satellite SST retrievals. The specific targeted applications (at NOAA NESDIS and EUMETSAT) include supporting the production of daily blended SST analyses and adjusting observations to common reference times and sampling depths.

Table 1
Summary of the Research Cruise Data Used in the Supplemental Model Testing

Cruise	Period	Resolution (min)	Quantity validated
DYNAMO	11/8/2011–11/28/2011	1	Sea snake (5 cm)–TSG (5 m)
Nauru	6/21/1999–6/26/1999	10	Tsnake (5 cm)
Kwajex	8/14/1999–8/18/1999		
Iceland-Madeira	6/30/2003–7/3/2003	10	Tskin (radiometric)–TSG (5 m)
St Maarten-Florida	8/29/2003–9/1/2003		
	9/12/2003–9/15/2003		
	9/26/2003–9/27/2003		
	10/5/2003–10/11/2003		
TAO	11/3/2003–11.13/2003		
	11/15/2003–11/18/2003		
Charleston-Barbados	2/14/2004–2/25/2004		
Barbados-Puerto Rico	3/2/2004–3/6/2004		
Puerto Rico-Charleston	4/1/2004–4/11/2004		
Charleston-Miami	9/28/2004–10/1/2004		
Chile-Brazil	1/21/2005–1/22/2005		
	2/10/2005–2/21/2005		
Woods Hole-Ponta Delgada	7/20/2005–7/21/2005		
Charleston-Miami	9/20/2005–9/24/2005		

For this application, a one-dimensional version of the model was run with independent forcing at each oceanic point on a 0.5° resolution grid extending between 60°N and 60°S latitude, consistent with geostationary satellite coverage. The model was run with a 5-min resolution for a 2-day period. Forcing data input at each time step was interpolated from the 6-hourly GFS and Wave Watch III data described in Section 2.3. All quantities with the exception of the solar flux were interpolated linearly between the analyzed values. Interpolation of the downwelling solar flux was performed using an estimated cloud fraction derived from the difference between the analyzed value and the theoretical clear-sky value so as to preserve the shape of the solar heating cycle. Examples of the forcing fields on the model grid are shown in Figure 1. The temperature and salinity profiles were initialized as constant values based on the SST at the gridpoint from the GFS analysis and a fixed salinity of 35.2 PSU. The diurnal warming magnitude was taken as the difference between the top layer of the model (a subskin temperature) and the modeled temperature at 5-m depth. The daily diurnal warming amplitude was then taken as the peak simulated value on the second day of the run (assuming initialization on the day prior). We note that this approach may miss a small component of diurnal warming present at 5-m depth and neglects any small amount of warming within the skin layer. The reference depth was selected, in part, for its consistency with other testing of the model against ship-based observations.

An example of the simulated diurnal warming amplitude for 1 July 2019 is shown in Figure 2 along with the satellite-derived estimates from Himawari-8, GOES-16, and Meteosat-11. The limited spatial extent of the diurnal amplitudes derived from the "profile" methodology of Wick and Castro (2020) is apparent, but these locations correspond to the most consistently clear conditions and are where the greatest diurnal warming would be expected. Regions with elevated diurnal warming in the satellite observations are generally seen to correspond with regions of warming from the model simulation. The regions of greatest simulated diurnal warming are largely constrained to banded regions of low wind speeds in the summer hemisphere (as expected) as well as in the Mediterranean Sea. Peak simulated warming approaches amplitudes of 5 K.

The broadest range of different potential model configurations was evaluated for the month of July 2019. The parameters adjusted included the turbulence closure constants, the background mixing value, enhancement factors for shear-induced mixing and wave breaking effects, and a gustiness factor. Tested values for the parameters are summarized in Table 2 and explained below. Two different sets of the turbulence closure constants,

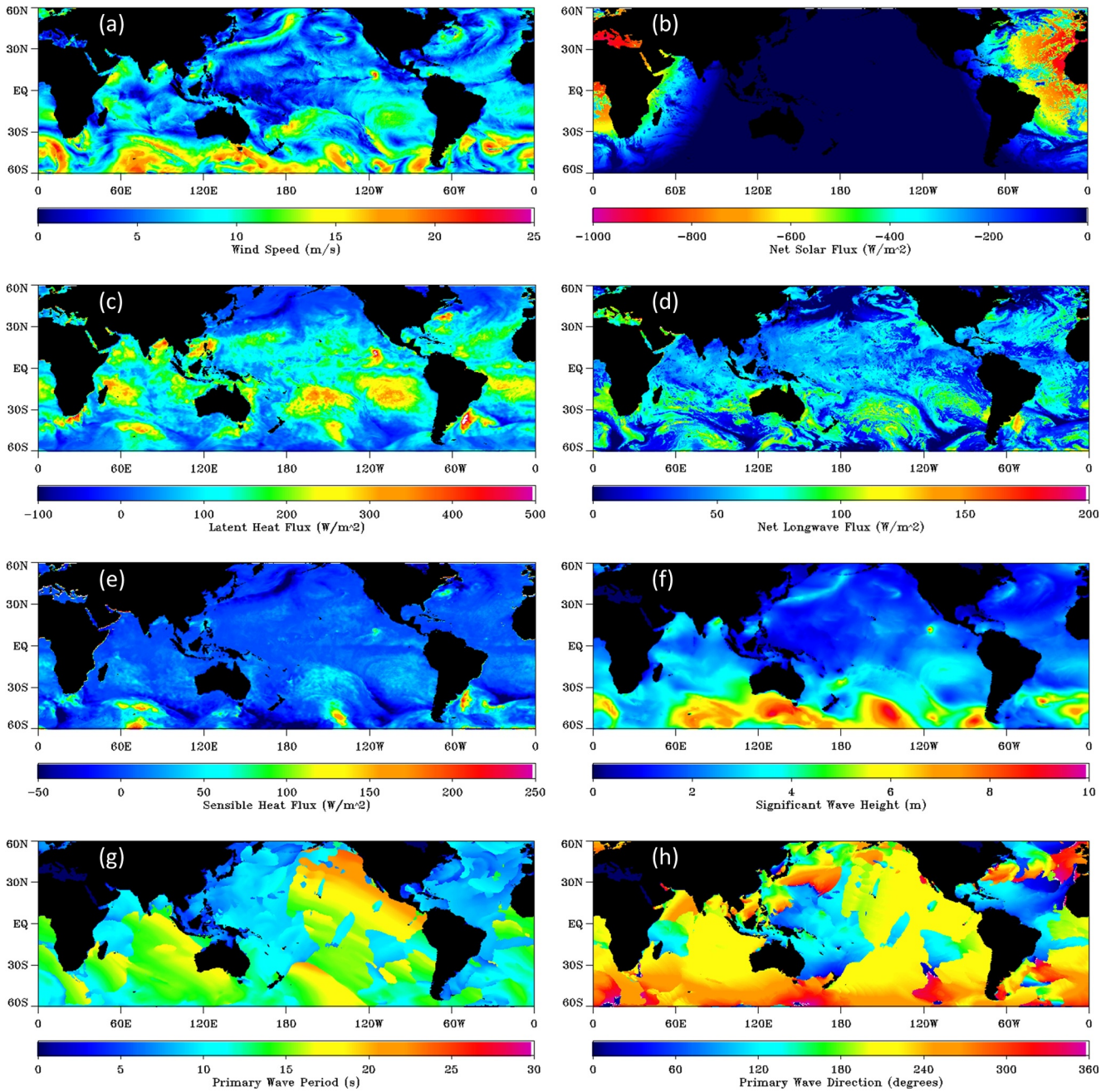

Figure 1. Maps of NWP-derived forcing fields for the gridded model taken from 12 Z on 1 July 2019. (a) The analysis fields from Global Forecast System include the wind speed, (b) net solar flux at the surface, (c) latent heat flux, (d) net longwave flux at the surface, and (e) sensible heat flux, (f) while the significant wave height, (g) primary wave period, and (h) primary wave direction are drawn from Wave Watch III outputs.

denoted as C1 and C2, were drawn from past publications on the model and previously shared code versions. Two different values of background mixing, K_{MB}, were also tested—one denoted as "base" consistent with previous general model application and some level of turbulent mixing, and one denoted "molecular" where the value is set to be consistent with molecular diffusion only. Two sets of the mixing enhancement factors were used, corresponding broadly to lower and higher degrees of enhancement. A wind gustiness factor was also added to the gridded model version to potentially compensate for extended periods of very low wind speeds introduced by coarse, 6-hr, NWP inputs and account for enhanced mixing introduced by short-duration wind gusts. The gustiness formulation was given by

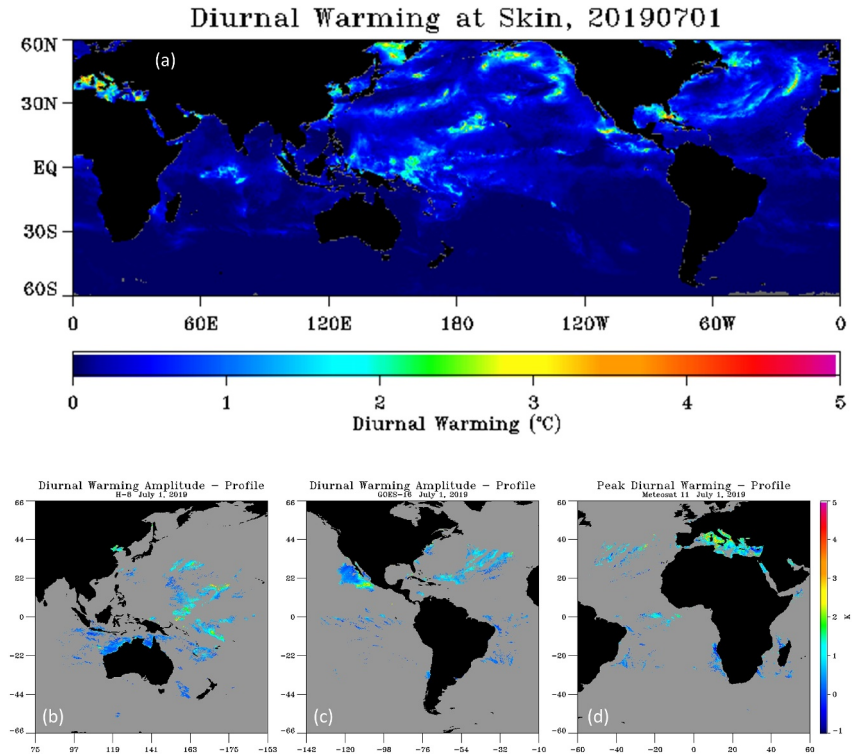

Figure 2. (a) Model-simulated diurnal warming amplitude for 1 July 2019 and (b) the corresponding satellite-derived amplitudes from Himawari-8, (c) GOES-16, and (d) Meteosat-11.

$$\tau = \left[\left(u^2 + G^2\right)/u^2\right] * \tau_0,$$

where τ is the wind stress, τ_0 the original wind stress, u is the wind speed and G is the gustiness factor. Three values of the parameter G were tested as shown in Table 2. Additional tests included turning off Langmuir mixing and wave breaking effects. Overall, 14 different combinations of these parameters were tested.

Table 2
Model Parameters Modified During the Testing of Different Configurations

Category	Designation	Values
Turbulent closure constants	C1	$(A_1, A_2, B_1, B_2) = (0.58, 0.62, 16.6, 12.04)$
		$(C_1, C_2, C_3) = (0.384, 0.7, 0.2)$
		$(E_1, E_2, E_3, E_4, E_5, E_6) = (1.8, 1.33, 1.0, 1.0, 0.0, 7.2)$
	C2	$(A_1, A_2, B_1, B_2) = (0.92, 0.74, 16.6, 10.1)$
		$(C_1, C_2, C_3) = (0.08, 0.7, 0.2)$
		$(E_1, E_2, E_3, E_4, E_5, E_6) = (1.8, 4.88, 1.8, 1.0, 0.0, 7.2)$
Background mixing	Base	$K_{HB} = 1.0E{-}5$
	Molecular	$K_{HB} = 8.8E{-}7$
Enhancement factors	Low	Shear enhancement factor = 1.0; wave enhancement = 10
	High	Shear enhancement factor = 2.0; wave enhancement = 100
Gustiness	None	$G = 0.0$
	Half	0.5
	Full	1.0

Table 3
Summary of Validation Statistics of the Different Model Configurations Relative to the Satellite-Derived Estimates

						GOES-16				Himawari-8				Meteosat-11			
Mod	Gust	Coef	Enh	Mix	Other	*N*	Bias	rms	*r*	*N*	Bias	rms	*r*	*N*	Bias	rms	*r*
KC	0	C1	High	Base		180,662	−0.11	0.37	0.73	152,470	−0.11	0.32	0.75	127,632	−0.25	0.57	0.60
		C2	Low	Base		180,662	0.19	0.55	0.74	152,470	0.15	0.49	0.76	127,632	0.00	0.64	0.59
		C1	Low	Base		180,662	0.16	0.53	0.74	152,470	0.12	0.48	0.76	127,632	−0.03	0.63	0.59
		C2	High	Base		180,662	−0.06	0.38	0.73	152,470	−0.08	0.32	0.75	127,632	−0.20	0.57	0.60
		C1	High	Mol		180,662	−0.08	0.46	0.69	152,470	−0.09	0.39	0.72	127,632	−0.19	0.80	0.53
		C2	Low	Mol		180,662	0.36	1.23	0.68	152,470	0.30	1.15	0.69	127,632	0.17	1.29	0.54
		C1	High	Base	NoL	180,662	−0.11	0.38	0.73	152,470	−0.11	0.32	0.75	127,632	−0.25	0.58	0.60
		C1	High	Base	NoW	180,662	0.04	0.47	0.75	152,470	0.04	0.42	0.76	127,632	−0.14	0.60	0.59
	0.5	C1	High	Base		180,662	−0.13	0.36	0.73	152,470	−0.14	0.32	0.76	127,632	−0.26	0.57	0.60
		C2	Low	Base		180,662	0.18	0.53	0.74	152,470	0.13	0.47	0.76	127,632	−0.01	0.62	0.59
		C1	High	Mol		180,662	−0.12	0.38	0.72	152,470	−0.13	0.32	0.75	127,632	−0.23	0.66	0.56
		C2	Low	Mol		180,662	0.30	0.97	0.70	152,470	0.24	0.90	0.71	127,632	0.11	1.04	0.56
	1	C1	High	Base		180,662	−0.17	0.38	0.71	152,470	−0.17	0.34	0.73	127,632	−0.30	0.56	0.59
		C2	Low	Base		180,662	0.13	0.46	0.74	152,470	0.08	0.40	0.75	127,632	−0.05	0.58	0.59
CO	1					179,919	−0.07	0.51	0.63	150,473	−0.09	0.40	0.69	126,376	−0.28	0.66	0.48
ZB						179,919	0.26	0.73	0.63	150,473	0.21	0.63	0.66	126,376	−0.01	0.77	0.43
TK						179,919	−0.31	0.49	0.61	150,473	−0.23	0.42	0.61	126,376	−0.55	0.78	0.24

Note. Mod: model type (KC = modified KC04, CO = COARE, TK = Takaya); Gust: gustiness factor; Coef: turbulence closure constants; Enh: mixing enhancement factor; Mix: background mixing (Mol-molecular). NoL = no Langmuir mixing; NoW = no wave breaking.

A full summary of the parameter combinations tested for July 2019 along with the corresponding statistics for comparison of the modeled and satellite-derived daily diurnal warming amplitudes for GOES-16, Himawari-8, and Meteosat-11 is shown in Table 3. Corresponding density-weighted scatter plots are shown in Figure 3 for several of the best-performing combinations relative to the GOES-16 observations. For the comparisons, the satellite-derived diurnal warming was first averaged over the matching 0.5° model grid cells to minimize any potential effect of differences in spatial resolution.

While the scatter plots and statistics reflect the correlation and centering around a "one-to-one" alignment between the highest density simulated and observed amplitudes, there is significant scatter observed for all of the approaches, particularly for the greatest amplitudes. A contribution to this scatter is the challenge of precisely capturing the regions of lowest wind speeds in the NWP forecast models. Slight differences in the alignment and positioning of the largest amplitude events can result in scatter and perfect one-to-one agreement is not expected. To reduce the sensitivity to these differences in positioning, additional insight can be obtained from comparisons of the frequency distributions of the diurnal warming amplitude. Comparisons of the distributions for a subset of the different model configurations are shown relative to those derived from the different geostationary satellites in Figure 4.

Considering all the comparisons together, the results obtained using the C1 coefficients, "base" background mixing, high mixing enhancement, and no gustiness (Figure 3a, line 1 in Table 2, and red trace in Figure 4) were among the best observed. The statistics alone show that different approaches yield the best values for different measures, but this model configuration results in a good overall combination and perhaps the best qualitative performance as viewed in Figures 3 and 4. This initial parameter combination was drawn from previous experimental testing against available cruise observations. More detailed validation against a larger set of research cruise observations is presented in Section 4.

The selection of the turbulence closure constants was found to have minimal impact on the simulated diurnal warming amplitudes (e.g., comparing Figures 3a and 3c, and red and green traces in Figure 4). This is reassuring given the challenge in determining definitive values associated with the closure assumptions. Additional tests

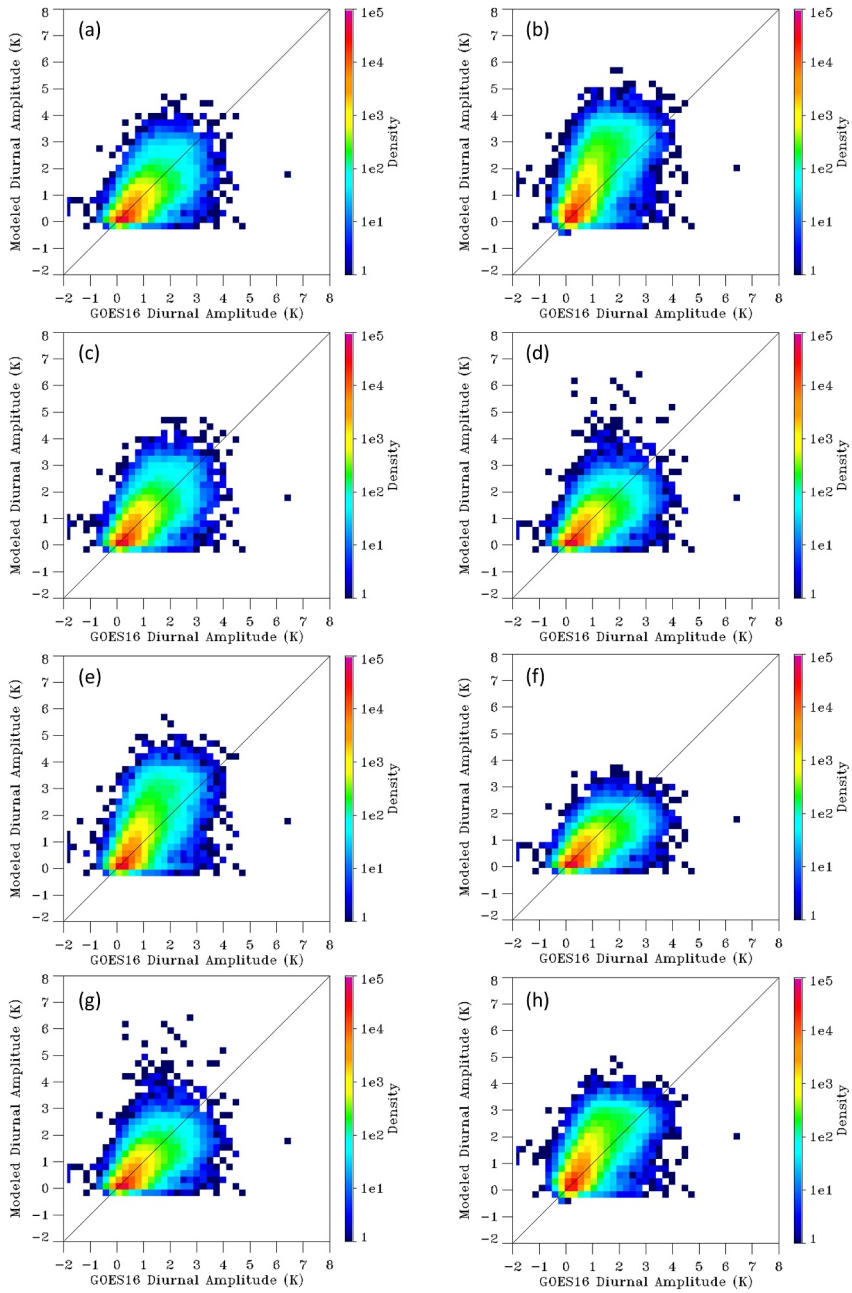

Figure 3. Density-weighted scatter plots comparing modeled daily diurnal warming amplitudes with estimates derived from GOES-16 compiled over the month of July 2019. (a) The presented configurations tested include no gustiness, C1 coefficients, high enhancement, and base background mixing; no gustiness, (b) C2 coefficients, low enhancement, base mixing; (c) no gustiness, C2 coefficients, high enhancement, base mixing; (d) no gustiness, C1 coefficients, high enhancement, molecular mixing; (e) no gustiness, C1 coefficients, no wave mixing, base background mixing; (f) half gustiness, C1 coefficients, high enhancement, base mixing; (g) half gustiness, C1 coefficients, high enhancement, molecular mixing; and (h) full gustiness, C2 coefficients, low enhancement, base mixing.

demonstrated that increasing the depth of the model domain from 50 to 200 m also did not have a significant impact on the simulated amplitudes and those results have not been included.

Greater sensitivity to the mixing enhancement factors and background mixing value was demonstrated. For the current model configuration and solar absorption parameterization, use of the lower mixing enhancement factors (e.g., Figure 3b) resulted in a tendency to overpredict the diurnal warming. Turning off wave effects (Figure 3e

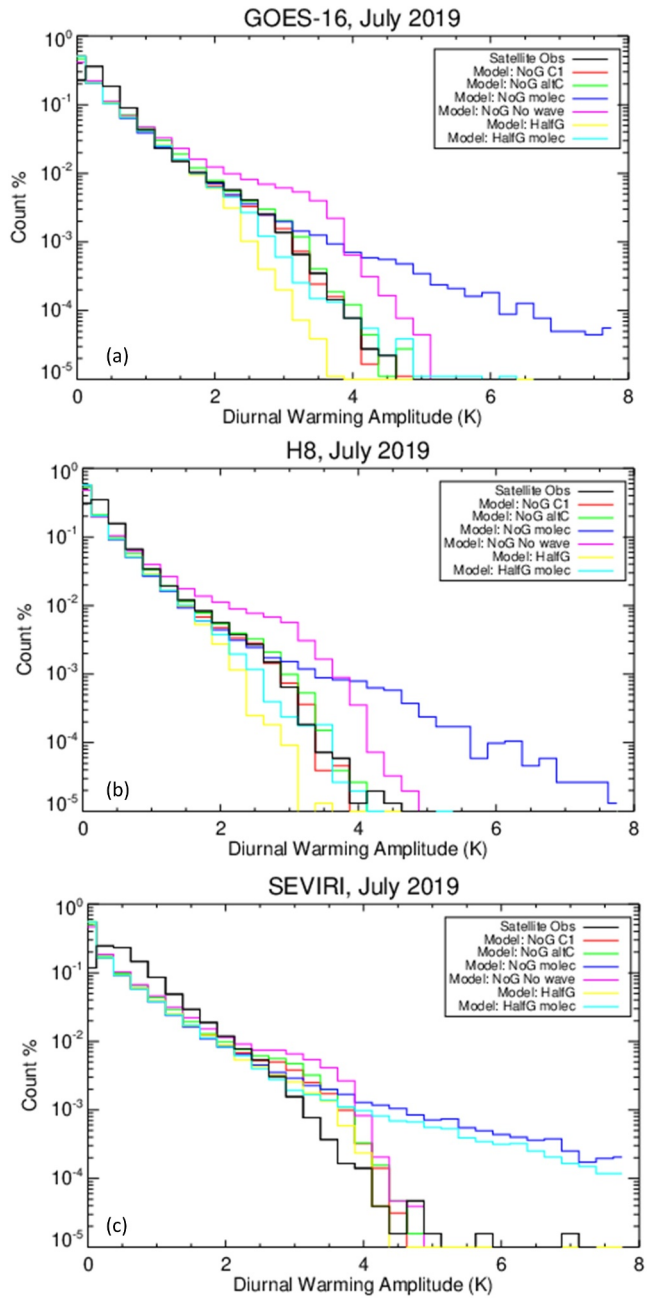

Figure 4. (a) Comparison of frequency distributions of the modeled daily diurnal warming amplitude with estimates derived from GOES-16, (b) Himawari-8, and (c) Meteosat-11 accumulated over the month of July 2019. The black trace represents the observations while the model configurations represented by the colored traces include: no gustiness, C1 coefficients, high enhancement, and base background mixing (red); no gustiness, C2 coefficients, high enhancement, and base background mixing (green); no gustiness, C1 coefficients, high enhancement, molecular mixing (blue); no gustiness, C1 coefficients, no wave mixing, base background mixing (magenta); half gustiness, C1 coefficients, high enhancement, base mixing (yellow); and half gustiness, C1 coefficients, high enhancement, molecular mixing (cyan).

and magenta trace in Figure 4) similarly resulted in a tendency to increase the diurnal warming amplitude too rapidly. Use of molecular background mixing (Figures 3d and 4 blue trace) resulted in amplification of the largest simulated diurnal warming beyond that observed with the satellite data. Additional fine tuning of the mixing enhancement factors and background mixing could be pursued to further improve agreement with the satellite observations, but the agreement with the identified combination above is generally favorable. In particular, reduced molecular mixing is not required to reproduce the larger observed diurnal warming amplitudes.

Introduction of gustiness was not required to achieve favorable simulations of the diurnal warming amplitude. The gustiness was added when previous testing using an earlier version of GFS forcing data suggested an overprediction of diurnal warming amplitudes at lower winds. The present testing demonstrates that in the current configuration, the use of appropriate parameter values can adequately limit the magnitude of warming. Use of gustiness did improve the scores relative to some statistical measures (like the standard deviation), but the gustiness may reduce the largest magnitude warming below what is observed.

Looking specifically at the distributions of diurnal warming amplitudes across all the satellites in Figure 4 shows that while the baseline configuration identified above reproduces the frequency of occurrence of the largest diurnal warming events relative to GOES-16 and Himawari-8 very well in July, the warming may be more overpredicted relative to the SEVIRI on Meteosat-11. The Meteosat-11 domain includes the Mediterranean Sea, which presents some unique modeling challenges including the lack of wave data in Wave Watch III, but previous results suggest some potential for the underestimation of the diurnal warming amplitude by SEVIRI for the largest amplitude events. Wick and Castro (2020), when examining overlapping diurnal warming estimates from GOES-16 and Meteosat-11, noted that the amplitudes from GOES-16 tended to be larger than coincident values from the SEVIRI for the largest events. This was potentially attributed to increased sensitivity of the GOES-16 SST retrieval algorithm relative to that for SEVIRI (Petrenko et al., 2019; Wick & Castro, 2020). Supplementing these results, point-by-point collocations between diurnal warming amplitudes from the satellites and drifting buoys suggest closer agreement for GOES-16 and Himawari-8 than for Meteosat-11 (not shown).

Given the favorable performance of the configuration using the C1 coefficients, "base" background mixing, high mixing enhancement, and no gustiness during the month of July, the testing was then extended to cover multiple seasons throughout the year. Comparisons of the frequency distributions of the diurnal warming amplitude and frequency-weighted scatter plots of the amplitude relative to combined observations from the GOES-16 and Himawari-8 satellites are shown in Figures 5 and 6, respectively for the months of July 2019, September 2019, January 2020, and March 2020. Corresponding predictions of the diurnal warming amplitude from the COARE, ZB, and Takaya et al. models were also derived for comparison. The results from each of the models have been added to Figure 5 while those from COARE and Takaya were added to Figure 6. Limited testing of other configurations for the modified KC04 model was also performed in the additional months but the relative performance of the configurations was similar to that for July 2019 and those results are not shown.

The selected configuration of the modified KC04 model is seen to also perform favorably in the months of March and September, particularly with regard to the frequency distributions. Its poorest performance is in January 2020 when the model underestimates some of the largest diurnal warming amplitudes. The COARE and ZB models deviate much more from a one-to-one centered agreement with the observed amplitudes and notably overestimate the largest diurnal warming amplitudes for this application with coarse resolution forcing. The Takaya model, in comparison, tends to slightly underestimate the largest diurnal warming amplitudes relative to the KC04 model and the observations. Given that the Takaya model was proposed as an improvement to ZB and the ZB overestimates were particularly large, only Takaya is shown in Figure 6.

Overall, the identified configuration of the modified KC04 model provides near-global estimates of the daily subskin diurnal warming amplitude based on NWP-forcing inputs that broadly align with the tendencies of observations and reproduce the frequency of occurrence of the largest amplitude diurnal warming events with good reliability. The model, in particular, performs better than the other models we considered. The derived amplitudes can potentially be applied to the combination of SST observations from different times and depths in blended SST analyses, but the associated uncertainty, particularly for specific location-based estimates must still be considered. The scatter apparent in the various direct comparisons demonstrates that this uncertainty is not negligible.

Basing a measure on the root mean square (rms) error statistics for the comparisons, an uncertainty of ~0.4 K in the predicted daily diurnal warming amplitude can be inferred using the preferred configuration if observations of all magnitudes are considered. This value, however, is comparable in magnitude to the mean overall observed diurnal warming amplitude. Of potentially greater value for application to the production of blended SST analyses is the uncertainty in the larger magnitude events. It is the adjustment of instantaneous observations during these events that are largest, most needed, and will have the biggest impact on the blended products. Additionally, observations during these events are often excluded entirely in production of some analyses. If comparison of the model- and satellite-derived amplitudes are constrained to cases where the observed amplitude exceeds 1 K, the

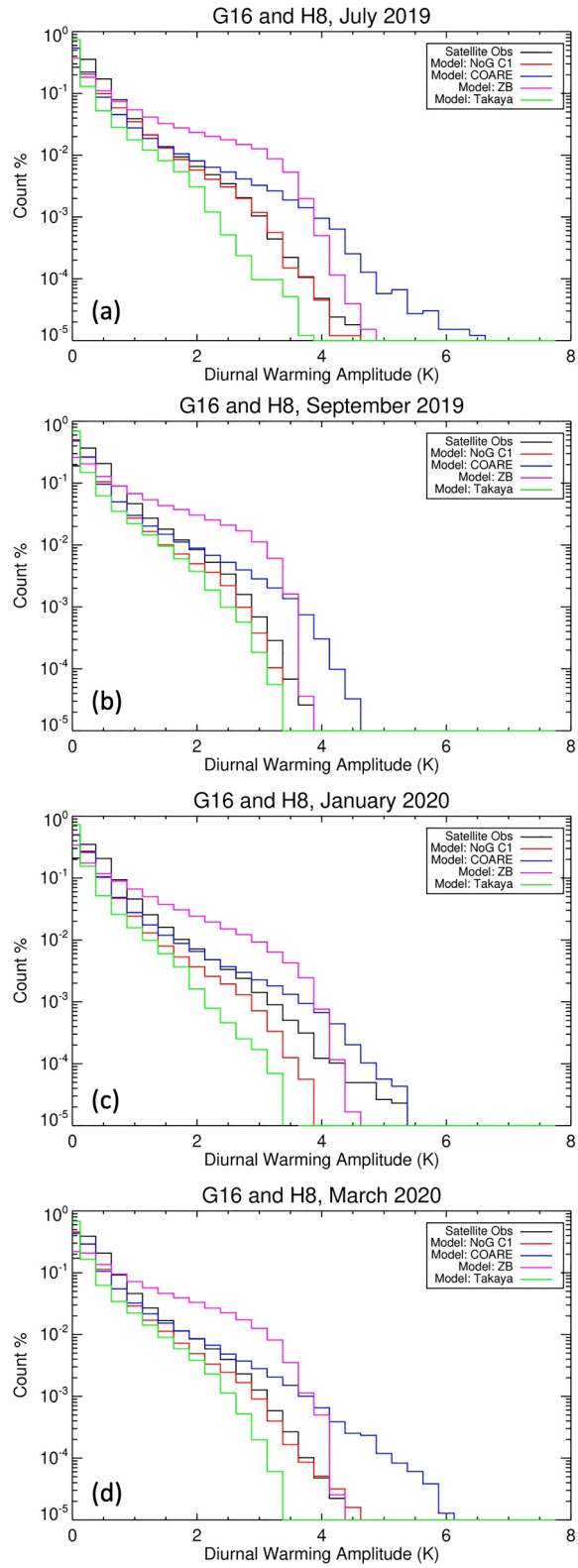

Figure 5. Comparisons of the satellite-derived diurnal warming frequency distribution (black) with simulations from the modified KC04 model with preferred configuration (red), COARE model (blue), ZB model (magenta), and Takaya model (green). Results were compiled from the GOES-16 and Himawari-8 satellites over the months of (a) July 2019, (b) September 2019, (c) January 2020, and (d) March 2020.

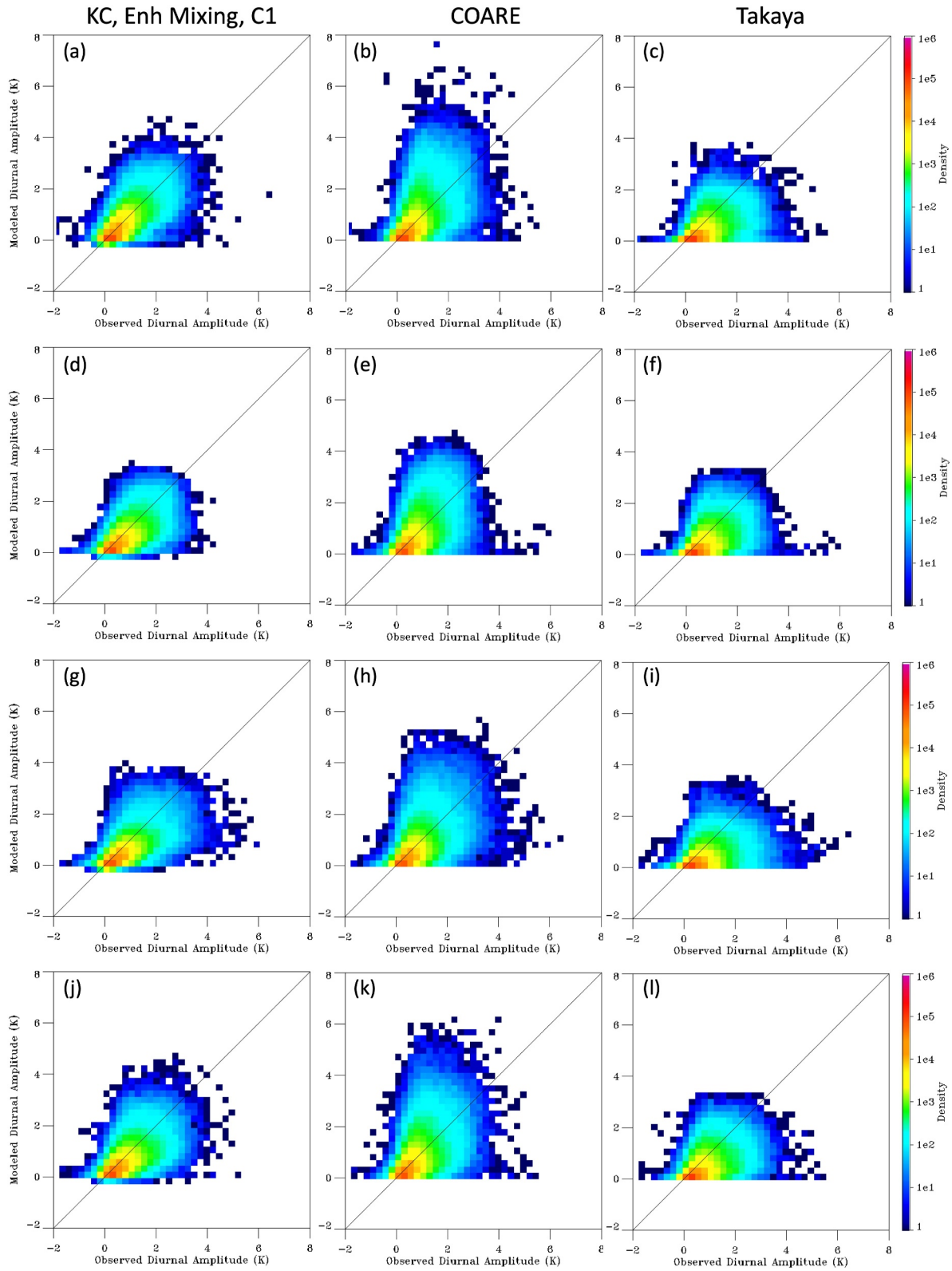

Figure 6. Density-weighted scatter plots comparing modeled daily diurnal warming amplitudes from the modified KC04 model (left column), COARE model (center column), and Takaya model (right column) with estimates derived from the GOES-16 and Himawari-8 satellites compiled over the months of July 2019 (top row), September 2019 (second row), January 2020 (third row), and March 2020 (bottom row).

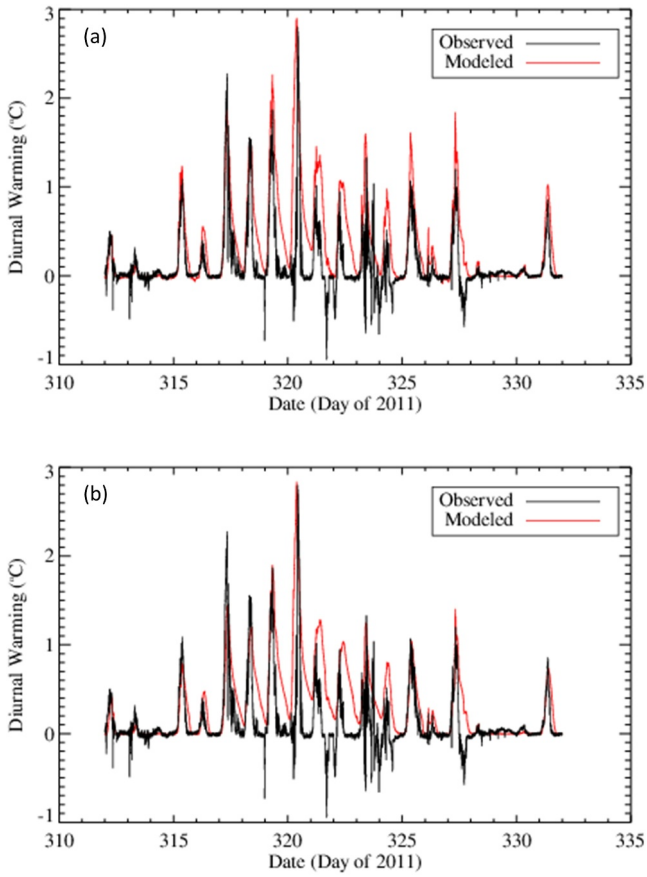

Figure 7. Comparison of the diurnal warming amplitude simulated using the modified KC04 model against direct observations from a cruise segment during the DYNAMO experiment. Panel (a) shows the simulated results using the preferred configuration from the gridded model simulations with the assumption of fully-developed seas while panel (b) shows results from a slightly modified configuration where available wave information was added, the Stokes drift is not inferred from the wind speed, and the shear enhancement factor was reduced from 2 to 1.

corresponding rms of the differences is ~0.7 K. For observed amplitudes in excess of 2 K, the uncertainty further rises to ~1 K. Such increases are expected given the nonlinearity of diurnal warming with wind speed. While these uncertainties are notable, particularly with respect to the desired accuracy of the blended SST analyses, they are less than the diurnal warming signal that might otherwise be ignored if no correction were attempted.

4. Independent Comparison Against High-Resolution Cruise Observations

The previous comparisons focused on evaluating whether an optimal configuration of the modified KC04 model could be identified that would yield reliable predictions of the diurnal warming over a near-global grid when forced with coarse NWP-derived forcing. While a potential configuration was found, it is important to assess whether this configuration is also consistent with, and suitable for, application to higher resolution cruise-based observations. Applications of this type are more consistent with the traditional utilization of the model and good performance of a common configuration would provide greater confidence in the validity of the model. In this section, the same model (configured with the C1 coefficients, "base" background mixing, high mixing enhancement, and no gustiness) is forced with and validated against data from several research cruises acquired over a wide range of times and conditions.

Tests were first conducted using observations from the DYNAMO field campaign during 2011. In this experiment focused on exploring the atmospheric and oceanic processes associated with the Madden-Julian oscillation (Yoneyama et al., 2013), observations of the near-surface temperature structure, wind stress, and heat fluxes were collected from the R/V *Revelle* in the equatorial Indian Ocean. Measurements at 1-min resolution were taken from the data set developed by Edson et al. (2016) from the period from 8 to 28 November 2011. This period has several days with significant diurnal warming amplitudes including one day with warming near 3 K. Giglio et al. (2017) previously demonstrated that the GOTM model exhibited good skill in reproducing the observed warming.

The modified KC04 model with the preferred configuration identified above but with a reduced 1-min time step was forced with the direct measurements and used to simulate the diurnal variation in the near-surface temperature profile. The 1-D model was driven with the observations following along the ship track and the simulated temperature profile shifted so that the 5-m temperature was fixed to the measurements from the ship's thermosalinograph. All wave-related parameters were derived from the wind speed assuming fully developed seas as for the previous experiment when wave model output was not available. The simulated diurnal warming is shown compared against observations derived from the difference between the sea-snake floating thermistor, with an effective depth of ~5 cm, and the ship's thermosalinograph, at a depth of ~5 m, in Figure 7. The results show that use of the identical model configuration yields simulated diurnal amplitudes (Figure 7a) that generally agree favorably with the observations, particularly for the 3 K warming event on 16 November. While the simulated warming agrees well on several days including 16 November, 11 November, and 27 November, there is a tendency for the amplitude to be overpredicted on other days, particularly the period from 17 to 23 November.

An additional run was performed in which available measurements of the significant wave height were used directly and the Stokes drift was not inferred from the wind speed. Additionally, the shear enhancement factor was reduced from 2 to 1. With this change, as reflected in the results in Figure 7b, the 3 K warming on 16 November is still accurately reproduced, but the peak amplitude on all the other days is now also well predicted. These results demonstrate that excellent agreement for this specific region can be achieved with the modified KC04 model and

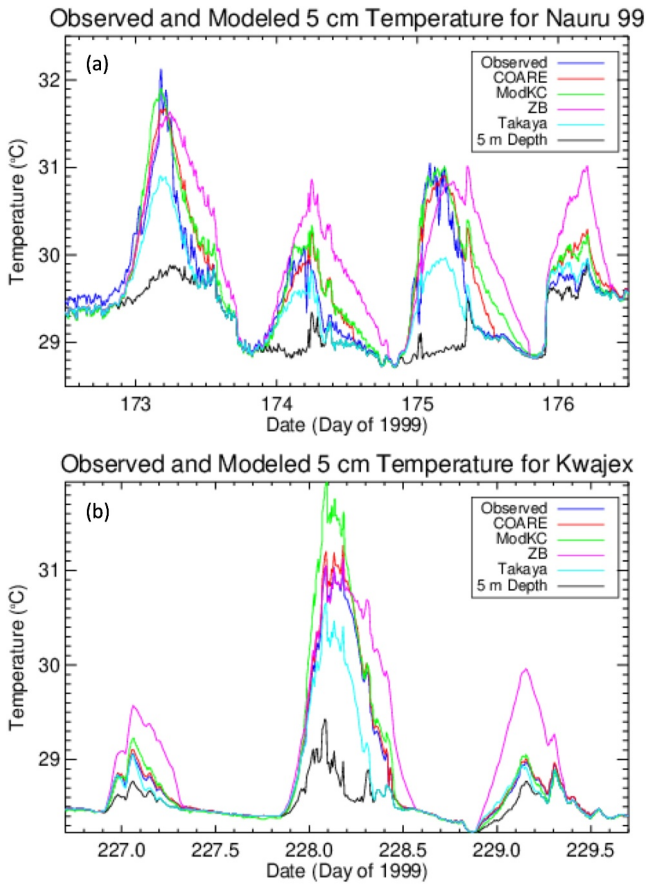

Figure 8. Comparison of the observed (blue trace) and simulated temperatures at 5-cm depth from the modified KC04 model (green), COARE model (red), ZB model (magenta), and Takaya model (cyan) for periods from the (a) Nauru and (b) Kwajex cruises in 1999. The observed temperature at 5-m depth is shown in black to highlight the amount of diurnal warming.

a small degree of extra tuning, but the general gridded model configuration performs reasonably well on its own. The differing performance associated with the two configurations could be related to the available wave data.

Additional testing was performed with short segments from older cruises contained within the historical marine and air-sea flux database developed and maintained by NOAA PSL and its predecessor ETL. The data set was instrumental in the development and testing of the COARE air-sea flux parameterization (Fairall, Bradley, Rogers, et al., 1996) and warm-layer model (Fairall, Bradley, Godfrey, et al., 1996). Simulations were performed for two periods with observed diurnal warming in excess of 1.5 K drawn from the Nauru and KWAJEX cruises in 1999. The preferred configuration from the gridded testing was again applied to the cruise data. For these cruises, the observations were at 10-min resolution but the model was run with a 1-min time step. While the testing against the DYNAMO data was unique to this study, the Nauru and KWAJEX data had been used to test versions of the Kantha-Clayson model previously and helped define the initial model configuration. The COARE and ZB models were also tested against these observations for comparison purposes.

In the results presented in Figure 8, the simulated temperatures at 5-cm depth are plotted along with the corresponding sea-snake thermistor measurements and the observations at 5-m depth used to drive the models. For these days, the COARE model reproduces the observed 5-cm temperatures very well and the modified KC04 model matches both the observations and COARE predictions on all but the second day of KWAJEX when the model overestimates the diurnal warming amplitude. The ZB model, in contrast, exhibits a greater tendency to overpredict the warming while the Takaya et al. (2010) model tends to underestimate the largest warming, consistent with the results from Section 3.

For a final test, the models were tested against an extended sequence of observations from the NOAA R/V *Ronald H. Brown* in 2003–2005 when radiometric skin temperature measurements were obtained with the CIRIMS (Jessup & Branch, 2008) by the APL at the University of Washington. Modeled warming was simulated relative to input observations of the temperature at ∼5-m depth. The models were run for 15 segments with observed instances of diurnal warming drawn from 10 cruise legs, as indicated in Table 1. Differences between the simulated and observed diurnal warming amplitudes, computed as the difference between the skin temperature and temperature at 5-m depth, were binned by the local solar time (LST). While the skin temperature is directly computed within the COARE combined warm layer/cool skin model, the skin layer parameterization from the COARE model (Fairall, Bradley, Godfrey, et al., 1996) was used to convert the top level (subskin) simulated temperature from the modified KC04 model to a skin temperature.

The results shown in Figure 9 present the bias and rms difference in the diurnal warming amplitude within each hourly time bin both for all the observations (Figure 9a) and only those cases where the wind speed was less than 4 m/s (Figure 9b) when diurnal warming is expected to be greater. Both the modified KC04 and COARE models show generally small biases for the simulated skin temperatures, particularly between 12 and 15 LST when the warming is expected to be most significant. For all wind speeds the bias in COARE is nearly zero while the modified KC04 model has a slight positive bias. At low wind speeds, however, the modified KC04 model bias is less during the period between 12 and 15 LST. The bias in the ZB model is much greater and shows more variation with the LST. The Takaya model exhibits a negative bias at the hours of peak warming, particularly at the low wind speeds. All models except Takaya exhibit a tendency to preserve the diurnal warming too late into the evening. This tendency is clearly evident for the modified KC04 model in both Figures 7 and 8 as well. While the bias in the amplitude of the simulated diurnal warming is quite small midday, the variability in the predictions as reflected by the rms error is again quite significant. For the lower wind speeds, this uncertainty approaches ∼1 K which can be similar to the amplitude of the diurnal warming.

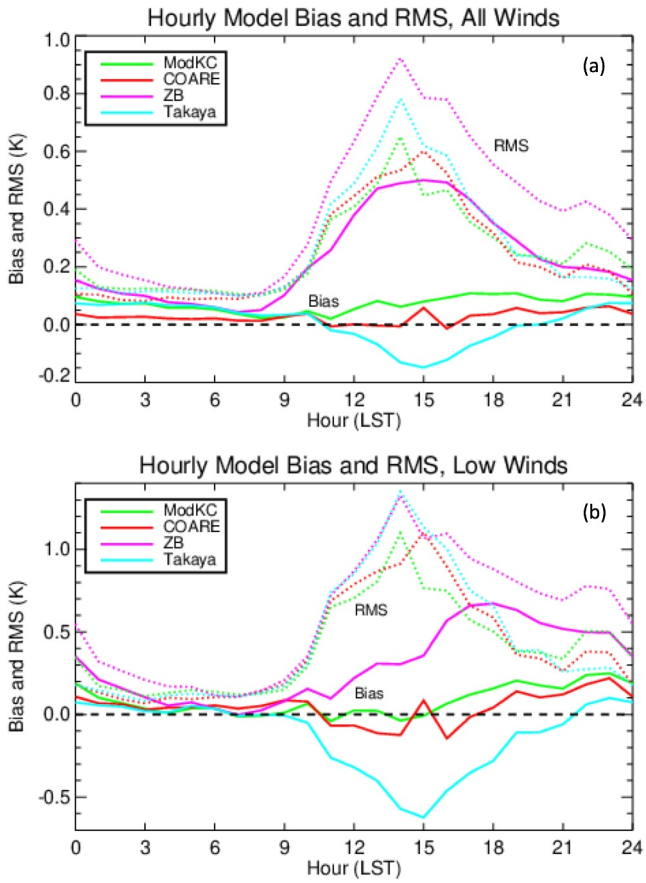

Figure 9. Hourly variation in the bias (solid lines) and rms errors (dotted lines) in the simulated diurnal warming relative to observations from 15 extracted cruise segments for the modified KC04 model (green), COARE model (red), ZB model (magenta), and Takay model (cyan). (a) Results are shown for the combination of all observations, and (b) only those were the instantaneous wind speed was less than 4 m/s.

5. Discussion and Conclusions

Multiple analyses were conducted to evaluate the accuracy and utility of predictions of diurnal warming using a modified version of the 1-D Kantha-Clayson model with wave effects (Kantha & Clayson, 2004). The primary targeted application was estimation of the diurnal warming amplitude on a global grid for use in the generation of blended, multi-sensor SST analyses. The model could be used both to compensate for the amount of warming present in individual observations at different times and depths for estimation of a daily reference value like the foundation temperature as well as to provide time-varying temperatures at a user-specified depth from an analyzed foundation temperature. For this purpose, the study focused on the quantitative evaluation of different potential model configurations when forced with coarse-resolution NWP model outputs from the NOAA GFS and Wave Watch III models. The accuracy of the simulated diurnal warming amplitudes was evaluated through comparison against estimates derived from operational SST retrievals from geostationary satellites. This specific application and evaluation of the modified KC04 model is unique in its focus on near-surface diurnal warming (as opposed to broader mixed layer characteristics) and the sensitivity analysis with respect to multiple model parameters.

The results indicated that application of the model with NWP forcing and a configuration using the C1 coefficients, "base" background mixing, high mixing enhancement, and no gustiness can capture the observed global (60°N–60°S) variations of the diurnal warming amplitude and, in particular, reproduce the frequency of occurrence of the largest amplitude diurnal warming events with reasonable reliability. The predicted amplitudes cluster around a direct one-to-one agreement with the observed amplitudes albeit with significant scatter. The agreement is generally preserved across all regions and seasons. The suitability and generality of the identified configuration is further supported through favorable reproduction of the observed diurnal warming amplitude from high-resolution research cruise-based observations using the same configuration.

While the model exhibits some skill in predicting diurnal warming amplitudes, even with only coarse-resolution NWP-based forcing, the associated uncertainties must be considered should one choose to use it. The uncertainty in the predicted warming at specific locations is significant. The more favorable reproduction of the frequency of occurrence of the diurnal warming amplitude relative to direct collocated amplitudes suggests issues with the positioning of the regions of lowest wind speeds in the NWP outputs. The model reproduces the appropriate range of amplitudes but potentially places them in the wrong locations. Even with accurate, high-resolution, observations from research cruises, however, notable uncertainty remains. The various experiments suggest an uncertainty near ∼1 K for the lowest wind speeds and largest diurnal warming amplitudes.

The identified configuration appears appropriate as a starting point for further application of the model for purposes aligned with those considered here. While past studies suggested a possible need for regional tuning, the selected configuration appears suitable for broader global application using similar forcing data. Additional optimization of the configuration parameters may, however, be desirable for specific applications or using significantly different forcing data. In particular, further sensitivity studies are recommended should alternate NWP-based forcing from the European Centre for Medium-Range Weather Forecasting (ECMWF) and/or at a higher temporal resolution be used. The results are also highly sensitive to the formulation used for the absorption of solar radiation with depth. Preliminary testing with an alternative approach that reduces the absorption at depths in the range between 1 and 5 m (not shown) suggests that reduced mixing rates would be required to produce similar favorable predictions of the diurnal warming. Ongoing work is continuing to explore these factors.

Though the gridded runs with NWP forcing were performed over 2-day periods, it is believed that the model need only be run at a given location from initialization during the prior nighttime. The 2-day period was selected in large part to facilitate application over the same period on a global grid with different local solar times. Further analyses could identify any sensitivity to the exact initialization time and run duration.

Use of the model in concert with additional information may be appropriate and lead to improved results. The tuning has generally resulted in matching the mean peak amplitude of the diurnal warming, but the warming consistently persists too long into the evening. As a result, simulated magnitudes of diurnal warming in the late afternoon and evening may be overestimated. This is a known issue of the model which is being explored further. In the interim, for the adjustment of observations to a common depth or time, it might be desirable to use a combination of the modeled diurnal warming amplitude superimposed on an idealized cycle of diurnal warming for times later in the day. A user might also wish to apply corrections only for larger magnitude diurnal warming events. For smaller events, the uncertainty can be comparable to the magnitude of warming itself. For larger events, the uncertainty typically increases but is less than the amplitude of diurnal warming. Additionally, it is these larger events that are most relevant to the production of blended SST analyses given the larger required adjustments to the individual observations.

While this study did not include a detailed comparison with the predictions of other candidate models for diurnal warming, the modified KC04 model did exhibit improved performance, at least on the global grid, relative to selected other models. While the COARE model performed well in the comparisons with high-resolution research cruise observations, it significantly overpredicted the diurnal warming amplitude when forced with the NWP outputs. The modified KC04 model exhibited greater flexibility in application to both coarse- and fine-resolution forcing. The ZB model overestimated the observed amplitudes in almost all tests. While Zhang et al. (2018) found these elevated values provided good agreement with observations from the MTSAT-1R satellite when retrieval sensitivity was considered, the results here relative to satellite retrievals with high sensitivity and other different observation types (as well earlier findings from Karagali and Høyer (2013)) suggest the predicted ZB amplitudes are too large. The Takaya et al. (2010) model developed to improve upon the ZB model tended to underestimate the observed warming in this study, though the values for the surface Stokes velocity derived under the assumption of fully developed seas for the cruise data sets may not be the most appropriate values.

Data Availability Statement

Operational NWP outputs were obtained from the NOAA National Centers for Environmental prediction at https://www.nco.ncep.noaa.gov/pmb/products/gfs/. Derived gridded inputs as applied in this study are available but have not been publicly hosted due to volume considerations. The Meteosat-11 SST data were downloaded from the NASA JPL PO.DAAC via their cloud data access point at https://podaac.jpl.nasa.gov/cloud-datasets/dataaccess. Satellite SST retrievals from GOES-16 and Himawari-8 were obtained by direct ftp from NOAA/NESDIS/STAR in near real time but can also be obtained from the PO.DAAC. Derived diurnal amplitudes are hosted by NOAA PSL at https://downloads.psl.noaa.gov/et6/sat/diurnal/geostationary_dw/. The DYNAMO cruise data was obtained through an archive maintained by the National Center for Atmospheric Research Earth Observing Laboratory (https://doi.org/10.5065/D6KP80J9) while the other cruise data were drawn from the archives at NOAA PSL at https://downloads.psl.noaa.gov/BLO/Air-Sea. The baseline version of the model code for the NWP-based inputs is shared at https://downloads.psl.noaa.gov/et6/sat/diurnal/src/.

Acknowledgments
This work was partially supported by funding from NOAA/NESDIS/STAR for development of their diurnally-compensated blended SST analysis as well as base funding from NOAA PSL. Additional contributions of SLC and AH were supported through NOAA grant NA19NES4320002. GAW gratefully acknowledges discussions and interactions with Lakshmi Kantha over the years regarding the use and modification of the Kantha-Clayson model. The efforts of Chris Fairall and his associates in collecting and compiling the cruise data are greatly appreciated. Data from the CIRIMS radiometer was graciously provided by Dr. Andrew Jessup from APL/UW. Constructive comments were provided by Dr. Elizabeth Thompson during internal review. The helpful comments of A. Pisano and another anonymous reviewer are also gratefully acknowledged.

References

Akella, S., Todling, R., & Suarez, M. (2017). Assimilation for skin SST in the NASA GEOS atmospheric data assimilation system. *Quarterly Journal of the Royal Meteorological Society*, *143*(703), 1032–1046. https://doi.org/10.1002/qj.2988

Bellenger, H., Takayabu, Y. N., Ushiyama, T., & Yoneyama, K. (2010). Role of diurnal warm layers in the diurnal cycle of convection over the tropical Indian Ocean during MISMO. *Monthly Weather Review*, *138*(6), 2426–2433. https://doi.org/10.1175/2010MWR3249.1

Bernie, D. J., Guilyardi, E., Madec, G., Slingo, J. M., & Woolnough, S. J. (2007). Impact of resolving the diurnal cycle in an ocean-atmosphere GCM. Part 1: A diurnally forced OGCM. *Climate Dynamics*, *29*(6), 575–590. https://doi.org/10.1007/s00382-007-0249-6

Bernie, D. J., Woolnough, S. J., Slingo, J. M., & Guilyardi, E. (2005). Modeling diurnal and intraseasonal variability of the ocean mixed layer. *Journal of Climate*, *18*(8), 1190–1202. https://doi.org/10.1175/jcli3319.1

Brasnett, B. (2008). The impact of satellite retrievals in a global sea-surface-temperature analysis. *Quarterly Journal of the Royal Meteorological Society*, *134*(636), 1745–1760. https://doi.org/10.1002/qj.319

Brunke, M. A., Zeng, X., Misra, V., & Beljaars, A. (2008). Integration of a prognostic sea surface skin temperature scheme into weather and climate models. *Journal of Geophysical Research*, *113*(D21), D21117. https://doi.org/10.1029/2008JD010607

Burchard, H., Bolding, K., & Villarreal, M. R. (1999). *GOTM—A general ocean turbulence model. Theory, applications and test cases. Technical Report EUR 18745 EN*. European Commission.

Castro, S. L., Wick, G. A., & Steele, M. (2016). Validation of satellite sea surface temperature analyses in the Beaufort Sea using UpTempO buoys. *Remote Sensing of Environment*, *187*, 458–475. https://doi.org/10.1016/j.rse.2016.10.035

Chin, T. M., Vazquez-Cuervo, J., & Armstrong, E. M. (2017). A multi-scale high-resolution analysis of global sea surface temperature. *Remote Sensing of Environment*, *200*, 154–169. https://doi.org/10.1016/.j.rse.2017.07.029

Clayson, C. A., & Bogdanoff, A. S. (2013). The effect of diurnal sea surface temperature warming on climatological air–sea fluxes. *Journal of Climate*, *26*(8), 2546–2556. https://doi.org/10.1175/JCLI-D-12-00062.1

Clayson, C. A., & Weitlich, D. (2007). Variability of tropical diurnal sea surface temperature. *Journal of Climate*, *20*(2), 334–352. https://doi.org/10.1175/jcli3999.1

Danabasoglu, G., Large, W. G., Tribbia, J. J., Gent, P. R., Briegleb, B. P., & McWilliams, J. C. (2006). Diurnal coupling in the tropical oceans of CCSM3. *Journal of Climate*, *19*(11), 2347–2365. https://doi.org/10.1175/jcli3739.1

Dash, P., Ignatov, A., Martin, M., Donlon, C., Brasnett, B., Reynolds, R., et al. (2012). Group for high resolution sea surface temperature (GHRSST) analysis fields intercomparisons. Part 2: Near-real time web-based level 4 SST quality monitor (L4-SQUAM). *Deep-Sea Research II*, *77–80*, 31–43. https://doi.org/10.1016/j.dsr2.2012.04.002

de Szoeke, S. P., Marke, T., & Brewer, W. A. (2021). Diurnal ocean surface warming drives convective turbulence and clouds in the atmosphere. *Geophysical Research Letters*, *48*(4), e2020GL091299. https://doi.org/10.1029/2020GL091299

Donlon, C., Robinson, I., Casey, K. S., Vasquez-Cuervo, J., Armstrong, E., Arino, O., et al. (2007). The global ocean data assimilation experiment high-resolution sea surface temperature pilot project. *Bulletin of the American Meteorological Society*, *88*(8), 1197–1213. https://doi.org/10.1175/bams-88-8-1197

Edson, J., Fairall, C., & de Szoeke, S. (2016). *R/V Roger Revelle Flux, Near-Surface Meteorology, and Navigation Data. Version 3.0*. UCAR/NCAR - Earth Observing Laboratory. https://doi.org/10.5065/D6KP80J9

Embury, O., Merchant, C. J., & Corlett, G. K. (2012). A reprocessing for climate of sea surface temperature from the along-track scanning radiometers: Initial validation, accounting for skin and diurnal variability effects. *Remote Sensing of Environment*, *116*, 62–78. https://doi.org/10.1016/j.rse.2011.02.028

Fairall, C. W., Bradley, E. F., Godfrey, J., Wick, G., Edson, J. B., & Young, G. (1996). Cool-skin and warm-layer effects on sea surface temperature. *Journal of Geophysical Research*, *101*(C1), 1295–1308. https://doi.org/10.1029/95JC03190

Fairall, C. W., Bradley, E. F., Rogers, D. P., Edson, J. B., & Young, G. S. (1996). Bulk parameterization of air-sea fluxes for TOGA-COARE. *Journal of Geophysical Research*, *101*(C2), 3747–3764. https://doi.org/10.1029/95jc03205

Flament, P., Firing, J., Sawyer, M., & Trefois, C. (1994). Amplitude and horizontal structure of a large sea surface warming event during the Coastal Ocean Dynamics Experiment. *Journal of Physical Oceanography*, *24*, 124–139.

Gentemann, C. L., Donlon, C. J., Stuart-Menteth, A., & Wentz, F. J. (2003). Diurnal signals in satellite sea surface temperature measurements. *Geophysical Research Letters*, *30*(3), 1140. https://doi.org/10.1029/2002GL016291

Gentemann, C. L., Minnett, P. J., Le Borgne, P., & Merchant, C. J. (2008). Multi-satellite measurements of large diurnal warming events. *Geophysical Research Letters*, *35*(22), L22602. https://doi.org/10.1029/2008GL035730

Gentemann, C. L., Minnett, P. J., & Ward, B. (2009). Profiles of Ocean Surface Heating (POSH): A new model of upper ocean diurnal warming. *Journal of Geophysical Research*, *114*(C7), C07017. https://doi.org/10.1029/2008JC004825

Giglio, D., Gille, S. T., Subramanian, A. C., & Nguyen, S. (2017). The role of wind gusts in upper ocean diurnal variability. *Journal of Geophysical Research: Oceans*, *122*(9), 7751–7764. https://doi.org/10.1002/2017JC012794

Good, S., Fiedler, E., Mao, C., Martin, M. J., Maycock, A., Reid, R., et al. (2020). The current configuration of the OSTIA system for operational production of foundation sea surface temperature and ice concentration analyses. *Remote Sensing*, *12*(4), 720. https://doi.org/10.3390/rs12040720

Hallsworth, S. (2005). *Modelling the diurnal variation of sea surface temperature using a one-dimensional ocean turbulence model* (PhD Thesis). University of Edinburgh.

Halpern, D., & Reed, R. K. (1976). Heat budget of the upper ocean under light winds. *Journal of Physical Oceanography*, *6*(6), 972–975. https://doi.org/10.1175/1520-0485(1976)006<0972:HBOTUO>2.0.CO;2

Ham, Y.-G., Kug, J.-S., Kang, I.-S., Jin, F.-F., & Timmermann, A. (2010). Impact of diurnal atmosphere-ocean coupling on tropical climate simulations using a coupled GCM. *Climate Dynamics*, *34*(6), 905–917. https://doi.org/10.1007/s00382-009-0586-8

Horrocks, L. A., Harris, A. R., & Saunders, R. W. (2003). *Modelling the diurnal thermocline for daytime bulk SST from AATSR. Forecasting Research Technical Report 418*. U.K. MetOffice Exeter.

Høyer, J. L., Le Borgne, P., & Eastwood, S. (2013). A bias correction method for Arctic satellite sea surface temperature observations. *Remote Sensing of Environment*, *146*, 201–213. https://doi.org/10.1016/j.rse.2013.04.020

Jessup, A. T., & Branch, R. (2008). Integrated ocean skin and bulk temperature measurements using the calibrated infrared in situ measurement system (CIRIMS) and through-hull ports. *Journal of Atmospheric and Oceanic Technology*, *25*(4), 579–597. https://doi.org/10.1175/2007JTECHO479.1

Kantha, L. H., & Clayson, C. A. (1994). An improved mixed layer model for geophysical applications. *Journal of Geophysical Research*, *99*(C12), 25235–25266. https://doi.org/10.1029/94JC02257

Kantha, L. H., & Clayson, C. A. (2004). On the effect of surface gravity waves on mixing in the oceanic mixed layer. *Ocean Modelling*, *6*(2), 101–124.

Karagali, I., & Høyer, J. L. (2013). Observations and modeling of the diurnal SST cycle in the North and Baltic Seas. *Journal of Geophysical Research: Oceans*, *118*(9), 4488–4503. https://doi.org/10.1002/jgrc.20320

Karagali, I., & Høyer, J. L. (2014). Characterization and quantification of regional diurnal SST cycles from SEVIRI. *Ocean Science*, *10*, 745–756.

Karagali, I., Høyer, J. L., & Donlon, C. J. (2017). Using a 1-D model to reproduce the diurnal variability of SST. *Journal of Geophysical Research: Oceans*, *122*(4), 2945–2959. https://doi.org/10.1002/2016JC012542

Kawai, Y., & Wada, A. (2007). Diurnal sea surface temperature variation and its impact on the atmosphere and ocean: A review. *Journal of Oceanography*, *63*(5), 721–744. https://doi.org/10.1007/s10872-007-0063-0

Kennedy, J. J., Brohan, P., & Tett, S. F. B. (2007). A global climatology of the diurnal variations in sea surface temperature and implications for MSU temperature trends. *Geophysical Research Letters*, *34*(5), L05712. https://doi.org/10.1029/2006GL028920

Large, W. G., & Caron, J. M. (2015). Diurnal cycling of sea surface temperature, salinity, and current in the CESM coupled climate model. *Journal of Geophysical Research: Oceans*, *120*(5), 3711–3729. https://doi.org/10.1002/2014JC010691

Le Borgne, P., Legendre, G., & Peré, S. (2012). Comparison of MSG/SEVIRI and drifting buoy derived diurnal warming estimates. *Remote Sensing of Environment*, *124*, 622–626. https://doi.org/10.1016/j.rse.2012.06.015

Li, W., Yu, R., Liu, H., & Yu, Y. (2001). Impacts of diurnal cycle of SST on the intraseasonal variation of surface heat flux over the Western Pacific warm pool. *Advances in Atmospheric Sciences*, *18*(5), 793–806. https://doi.org/10.1007/bf03403503

Luo, B., Minnett, P. J., Szczodrak, M., & Akella, S. (2022). Regional and seasonal variability of the oceanic thermal skin effect. *Journal of Geophysical Research: Oceans*, *127*(5), e2022JC018465. https://doi.org/10.1029/2022JC018465

Martin, M., Dash, P., Ignatov, A., Banzon, V., Beggs, H., Brasnett, B., et al. (2012). Group for high resolution sea surface temperature (GHRSST) analysis fields inter-comparisons. Part 1: A GHRSST multi-product ensemble (GMPE). *Deep-Sea Research II*, *77–80*, 21–30. https://doi.org/10.1016/j.dsr2.2012.04.013

Marullo, S., Minnett, P. J., Santoleri, R., & Tonani, M. (2016). The diurnal cycle of sea-surface temperature and estimation of the heat budget of the Mediterranean Sea. *Journal of Geophysical Research: Oceans*, *121*(11), 8351–8367. https://doi.org/10.1002/2016jc012192

Masson, S., Terray, P., Madec, G., Luo, J.-J., Yamagata, T., & Takahashi, K. (2012). Impact of intra-daily SST variability on ENSO characteristics in a coupled model. *Climate Dynamics*, *39*(3–4), 681–707. https://doi.org/10.1007/s00382-011-1247-2

Maturi, E., Harris, A., Mittaz, J., Sapper, J., Wick, G., Zhu, X., & Koner, P. (2017). A new high resolution sea surface temperature blended analysis. *Bulletin of the American Meteorological Society*, *98*(5), 1015–1026. https://doi.org/10.1175/bams-d-15-00002.1

McCreary, J. P., Jr., Kohler, K. E., Hood, R. R., Smith, S., Kindle, J., Fischer, A. S., & Weller, R. A. (2001). Influences of diurnal and intraseasonal forcing on mixed-layer and biological variability in the central Arabian Sea. *Journal of Geophysical Research*, *106*(C4), 7139–7155. https://doi.org/10.1029/2000jc900156

Mellor, G. L., & Yamada, T. (1974). A hierarchy of turbulence closure models for planetary boundary layers. *Journal of Atmospheric Science*, *31*(7), 1791–1806. https://doi.org/10.1175/1520-0469(1974)031<1791:ahotcm>2.0.co;2

Mellor, G. L., & Yamada, T. (1982). Development of a turbulence closure model for geophysical fluid problems. *Reviews of Geophysics and Space Physics*, *20*(4), 851–875. https://doi.org/10.1029/rg020i004p00851

Merchant, C. J., Embury, O., Bulgin, C. E., Block, T., Corlett, G. K., Fiedler, E., et al. (2019). Satellite-based time-series of sea-surface temperature since 1981 for climate applications. *Scientific Data*, *6*(1), 223. https://doi.org/10.1038/s41597-019-0236-x

Merchant, C. J., Filipiak, M. J., Le Borgne, P., Roquet, H., Autret, E., Piolle, J.-F., & Lavender, S. (2008). Diurnal warm-layer events in the western Mediterranean and European shelf seas. *Geophysical Research Letters*, *35*(4), L04601. https://doi.org/10.1029/2007gl033071

Noh, Y., & Kim, H. J. (1999). Simulations of temperature and turbulence structure of the oceanic boundary layer with the improved near-surface process. *Journal of Geophysical Research: Oceans*, *15*, 621–634. https://doi.org/10.1029/1999JC900068

Paulson, C. A., & Simpson, J. J. (1981). The temperature difference across the cool skin of the ocean. *Journal of Geophysical Research*, *86*(C11), 11044–11054. https://doi.org/10.1029/JC0086iC11p11044

Petrenko, B., Ignatov, A., Kihai, Y., & Pennybacker, M. (2019). Optimization of sensitivity of GOES-16 ABI sea surface temperature by matching satellite observations with L4 analysis. *Remote Sensing*, *11*(2), 206. https://doi.org/10.3390/rs11020206

Pimentel, S., Haines, K., & Nichols, N. K. (2008). Modeling the diurnal variability of sea surface temperatures. *Journal of Geophysical Research*, *113*(C11), C11004. https://doi.org/10.1029/2007JC004607

Pimentel, S., Tse, W.-H., Xu, H., Denaxa, D., Jansen, E., Korres, G., et al. (2019). Modeling the near-surface diurnal cycle of sea surface temperature in the Mediterranean Sea. *Journal of Geophysical Research: Oceans*, *124*(1), 171–183. https://doi.org/10.1029/2018JC014289

Pisano, A., Ciani, D., Marullo, S., Santoleri, R., & Buongiorno Nardelli, B. (2022). A new operational Mediterranean diurnal optimally interpolated sea surface temperature product within the Copernicus Marine Service. *Earth System Science Data*, *14*(9), 4111–4128. https://doi.org/10.5194/essd-14-4111-2022

Price, J. F., Weller, R. A., Bowers, C. M., & Briscoe, M. G. (1987). Diurnal response of sea surface temperature observed at the long-term upper ocean study (34°N, 70°W) in the Sargasso Sea. *Journal of Geophysical Research*, *92*(C13), 14480–14490. https://doi.org/10.1029/JC092iC13p14480

Price, J. F., Weller, R. A., & Pinkel, R. (1986). Diurnal cycling: Observations and models of the upper ocean response to diurnal heating, cooling, and wind mixing. *Journal of Geophysical Research*, *91*(C7), 8411–8427. https://doi.org/10.1029/JC091iC07p08411

Seo, H., Subramanian, A. C., Miller, A. J., & Cavanaugh, N. R. (2014). Coupled impacts of the diurnal cycle of sea surface temperature on the Madden-Julian oscillation. *Journal of Climate*, *27*(22), 8422–8443. https://doi.org/10.1175/jcli-d-14-00141.1

Shackelford, K., DeMott, C. A., van Leeuwen, P. J., Thompson, E., & Hagos, S. (2022). Rain-induced stratification of the equatorial Indian ocean and its potential feedback to the atmosphere. *Journal of Geophysical Research: Oceans*, *127*(3), e2021JC018025. https://doi.org/10.1029/2021JC018025

Shinoda, T. (2005). Impact of the diurnal cycle of solar radiation on intraseasonal SST variability in the western equatorial Pacific. *Journal of Climate*, *18*(14), 2628–2636. https://doi.org/10.1175/jcli3432.1

Shinoda, T., & Hendon, H. H. (1998). Mixed layer modeling of intraseasonal variability in the tropical western Pacific and Indian Oceans. *Journal of Climate*, *11*(10), 2668–2685. https://doi.org/10.1175/1520-0442(1998)011<2668:mlmoiv>2.0.co;2

Stuart-Menteth, A. C., Robinson, I. S., & Challenor, P. G. (2003). A global study of diurnal warming using satellite-derived sea surface temperature. *Journal of Geophysical Research*, *108*(C5), 3155. https://doi.org/10.1029/2002JC001534

Takaya, Y., Bidlot, J.-R., Beljaars, A. C. M., & Janssen, P. A. E. M. (2010). Refinements to a prognostic scheme of skin sea surface temperature. *Journal of Geophysical Research*, *115*(C6), C06009. https://doi.org/10.1029/2009JC005985

Thompson, E. J., Moum, J. N., Fairall, C. W., & Rutledge, S. A. (2019). Wind limits on rain layers and diurnal warm layers. *Journal of Geophysical Research: Oceans*, *124*(2), 897–924. https://doi.org/10.1029/2018JC014130

Tian, F., von Storch, J.-S., & Hertwig, E. (2019). Impact of SST diurnal cycle on ENSO asymmetry. *Climate Dynamics*, *52*(3–4), 2399–2411. https://doi.org/10.1007/s00382-018-4271-7

Tolman, H. L., Balasubramaniyan, B., Burroughs, L. D., Chalikov, D. V., Chao, Y. Y., Chen, H. S., & Gerald, V. V. (2002). Development and implementation of wind-generated ocean surface wave models. *Weather and Forecasting*, *17*(2), 311–333. https://doi.org/10.1175/1520-0434(2002)017<0311:daiowg>2.0.co;2

Vazquez-Cuervo, J., Castro, S., Steele, M., Gentemann, C., Gomez-Valdes, J., & Tang, W. (2022). Comparison of GHRSST SST analysis in the Arctic Ocean and Alaskan coastal waters using Saildrones. *Remote Sensing*, *14*(3), 692. https://doi.org/10.3390/rs14030692

Webster, P. J., Clayson, C. A., & Curry, J. A. (1996). Clouds, radiation, and the diurnal cycle of sea surface temperature in the tropical western Pacific. *Journal of Climate*, *9*(8), 1712–1730. https://doi.org/10.1175/1520-0442(1996)009<1712:CRATDC>2.0.CO;2

Weihs, R. R., & Bourassa, M. (2014). Modeled diurnally varying sea surface temperatures and their influence on surface heat fluxes. *Journal of Geophysical Research: Oceans*, *119*(7), 4101–4123. https://doi.org/10.1002/2013JC009489

While, J., Mao, C., Martin, M. J., Roberts-Jones, J., Sykes, P. A., Good, S. A., & McLaren, A. J. (2017). An operational analysis system for the global diurnal cycle of sea surface temperature: Implementation and validation. *Quarterly Journal of the Royal Meteorological Society*, *143*(705), 1787–1803. https://doi.org/10.1002/qj3036

Wick, G. A., Bates, J. J., & Scott, D. J. (2002). Satellite and skin layer effects on the accuracy of sea surface temperature measurements from the GOES Satellites. *Journal of Atmospheric and Oceanic Technology*, *19*(11), 1834–1848. https://doi.org/10.1175/1520-0426(2002)019<1834:sasleo>2.0.co;2

Wick, G. A., & Castro, S. L. (2020). Assessment of extreme diurnal warming in operational geosynchronous satellite sea surface temperature products. *Remote Sensing*, *12*(22), 3771. https://doi.org/10.3390/rs12223771

Wick, G. A., Ohlmann, J. C., Fairall, C. W., & Jessup, A. T. (2005). Improved oceanic cool-skin corrections using a refined solar penetration model. *Journal of Physical Oceanography*, *35*(11), 1986–1996. https://doi.org/10.1175/jpo2803.1

Woolnough, S. J., Vitart, F., & Balmaseda, M. A. (2007). The role of the ocean in the Madden-Julian Oscillation: Implications for MJO prediction. *Quarterly Journal of the Royal Meteorological Society*, *133*(622), 117–128. https://doi.org/10.1002/qj.4

Yang, G., & Slingo, J. (2001). The diurnal cycle in the tropics. *Monthly Weather Review*, *129*(4), 784–801. https://doi.org/10.1175/1520-0493(2001)129<0784:tdcitt>2.0.co;2

Yoneyama, K., Zhang, C., & Long, C. N. (2013). Tracking pulses of the Madden-Julian oscillation. *Bulletin of the American Meteorological Society*, *94*(12), 1871–1891. https://doi.org/10.1175/BAMS-D-12-00157.1

Zeng, X., & Beljaars, A. (2005). A prognostic scheme of sea surface skin temperature for modeling and data assimilation. *Geophysical Research Letters*, *32*(14), L14605. https://doi.org/10.1029/2005GL023030

Zhang, H., Beggs, H., Merchant, C. J., Wang, X. H., Majewski, L., Kiss, A. E., et al. (2018). Comparison of SST diurnal variation models over the tropical warm pool region. *Journal of Geophysical Research: Oceans*, *123*(5), 3467–3488. https://doi.org/10.1029/2017JC013517

Zhou, X., Zhu, Y., Hou, D., Fu, B., Li, W., Guan, H., et al. (2022). The development of the NCEP Global Ensemble Forecast System Version 12, Operational Prediction System Notes. *Weather and Forecasting*, *37*(6), 1069–1084. https://doi.org/10.1175/WAF-D-21-0112.1